Am J Physiol Cell Physiol 327: C462–C476, 2024.
First published June 24, 2024; doi:10.1152/ajpcell.00123.2024

american physiological society

AMERICAN JOURNAL OF PHYSIOLOGY
CELL PHYSIOLOGY

RESEARCH ARTICLE

β-Cell keratin 8 maintains islet mechanical integrity, mitochondrial ultrastructure, and β-cell glucose transporter 2 plasma membrane targeting

Sarah Baghestani,[1,2] Caroline Haldin,[1,2]* Petar Kosijer,[1,2]* Catharina M. Alam,[3]* and Diana M. Toivola[1,2,4]*

[1]*Cell Biology, Biosciences, Faculty of Science and Engineering, Åbo Akademi University, Turku, Finland;* [2]*InFLAMES Research Flagship, Åbo Akademi University, Turku, Finland;* [3]*School of Applied Sciences, Edinburgh Napier University, Edinburg, United Kingdom; and* [4]*Turku Center for Disease Modeling, University of Turku, Turku, Finland*

Abstract

Islet β-cell dysfunction is an underlying factor for type I diabetes (T1D) development. Insulin sensing and secretion are tightly regulated in β-cells at multiple subcellular levels. The epithelial intermediate filament (IF) protein keratin (K) 8 is the main β-cell keratin, constituting the filament network with K18. To identify the cell-autonomous functions of K8 in β-cells, mice with targeted deletion of β-cell K8 ($K8^{flox/flox}$; Ins-Cre) were analyzed for islet morphology, ultrastructure, and integrity, as well as blood glucose regulation and streptozotocin (STZ)-induced diabetes development. Glucose transporter 2 (GLUT2) localization was studied in β-cells in vivo and in MIN6 cells with intact or disrupted K8/K18 filaments. Loss of β-cell K8 leads to a major reduction in K18. Islets without β-cell K8 are more fragile, and these β-cells display disjointed plasma membrane organization with less membranous E-cadherin and smaller mitochondria with diffuse cristae. Lack of β-cell K8 also leads to a reduced glucose-stimulated insulin secretion (GSIS) response in vivo, despite undisturbed systemic blood glucose regulation. $K8^{flox/flox}$, Ins-Cre mice have a decreased sensitivity to STZ compared with K8 wild-type mice, which is in line with decreased membranous GLUT2 expression observed in vivo, as GLUT2 is required for STZ uptake in β-cells. In vitro, MIN6 cell plasma membrane GLUT2 is rescued in cells overexpressing K8/K18 filaments but mistargeted in cells with disrupted K8/K18 filaments. β-Cell K8 is required for islet and β-cell structural integrity, normal mitochondrial morphology, and GLUT2 plasma membrane targeting, and has implications on STZ sensitivity as well as systemic insulin responses.

NEW & NOTEWORTHY Keratin 8 is the main cytoskeletal protein in the cytoplasmic intermediate filament network in β-cells. Here for the first time, we assessed the β-cell autonomous mechanical and nonmechanical roles of keratin 8 in β-cell function. We demonstrated the importance of keratin 8 in islet and β-cell structural integrity, maintaining mitochondrial morphology and GLUT2 plasma membrane targeting.

β-cell ultrastructure; GLUT2; intermediate filament; islet integrity; keratin

INTRODUCTION

Maintaining blood glucose homeostasis in diabetes is metabolically demanding on pancreatic islet β-cells due to the constant requirement for insulin synthesis and secretion. The ability to meet this demand depends on the number of β-cells, their adaptive capacity, and functional integrity (1, 2). Due to their critical function in glucose sensing and insulin secretion, β-cells are highly susceptible to diabetes-related cell stress. Disruptions or insufficiencies in β-cell processes can affect β-cell mass and function and lead to alterations in systemic normoglycemia and increased diabetes susceptibility (3, 4). Cytoskeletal filament proteins are structural components in β-cells and contribute to several cellular processes. Actin microfilaments and microtubules have established roles in glucose and insulin processes through modulating glucose uptake (5) and the spatial organization, trafficking, and secretion of insulin granules (6, 7). It has been suggested that the β-cell cytoskeletal component, keratin intermediate filaments (IFs), also plays a role in β-cell glucose sensing, insulin secretion, and stress mechanisms (8). However, the β-cell autonomous functions of keratins are not known.

The epithelial keratin protein family forms filaments that consist of obligate heteropolymers of type I (K9-28) and type II (K1-8 and K71-80) keratins (9). Keratins are expressed in a cell-, development- and differentiation-dependent manner (10), have well-established stress-protecting functions in several organs, and are frequently upregulated during stress or regeneration (11, 12). Keratin filaments maintain mechanical stability in epithelial tissue by providing cells with structural support, for example, through binding by cytolinkers to

*C. Haldin and P. Kosijer contributed equally to this work. C. M. Alam and D. M. Toivola contributed equally to this work.
Correspondence: D. M. Toivola (diana.toivola@abo.fi).
Submitted 21 February 2024 / Revised 31 May 2024 / Accepted 12 June 2024

other cytoskeletal proteins, hemidesmosomes, or desmosomes (10, 13, 14). Keratins are organizers of the cytoplasmic space and are involved in several cellular processes such as targeting proteins and organelles, modulating signaling pathways, cell growth, proliferation, differentiation, and apoptosis (11, 15, 16). Simple epithelial tissues, such as the pancreas, liver, and intestine, express the type II K7 and K8 and type I K18–K20 and K23 keratins (17), where K8 is the main type II keratin in these tissues (18–20). K8 and K18 are the only keratins that are known to be expressed in human β-cells; however, mouse β-cells additionally express K7 (19, 21). Of interest, during experimental diabetes cell stress in several type I diabetes (T1D) mouse models, β-cell K7, K8, and K18 levels, and the filament network density increase significantly (8, 21).

The few studies so far addressing the roles of K8/K18 in β-cells and glucose homeostasis by gene deletion have used the global $K8^{-/-}$ mouse model. This model, however, has shown to be inadequate for studying β-cell mechanisms due to the multiorgan effects of systemic K8 deletion. Considering the major role of K8 in most simple epithelia, $K8^{-/-}$ mice present multiple pathologies in organs involved in glucose and insulin homeostasis and suffer from liver fragility and colitis (20, 22–24). $K8^{-/-}$ mice show alterations in systemic glucose use and insulin responses, whereas the β-cell insulin vesicle ultrastructure is irregular, and the overall insulin content and mitochondrial energy metabolism are reduced (8, 25). Nonetheless, it is unclear if these changes in $K8^{-/-}$ mice are specifically caused by K8 loss in β-cells or an indirect effect of increased β-cell stress due to disruptions in glucose metabolism and systemic inflammation owing to the liver and intestinal pathologies.

In this study, we hypothesized that K8 is important for β-cell function, and we aimed to identify the β-cell specific role of K8 in β-cell processes and diabetes sensitivity using a conditional β-cell K8 knockout mouse generated by the loxP-Cre-mediated system, under the insulin promotor. Our results show that β-cell K8 is specifically involved in maintaining islet structural integrity, insulin responses to glucose stimulation, mitochondrial morphology, and glucose transporter 2 (GLUT2) plasma membrane targeting.

MATERIALS AND METHODS

Experimental Animals

$K8^{flox/flox}$ transgenic mice, generated by, and a kind gift from, Prof. Karen Ridge (Northwestern University), in the C57BL/6 background (26), were used to generate a β-cell specific K8 knockout mouse. To achieve this, $K8^{flox/flox}$ were bred with female $Ins1^{Cre}$ (here called Ins-Cre) mice (27) (Jackson Laboratory/RRID:IMSR_JAX:026801) and backcrossed for at least six generations to minimize any potential differences between parental C57BL/6 strains. The conditional knockout mice were subsequently maintained by breeding $K8^{flox/flox}$ with $K8^{flox/flox}$; Ins-Cre. As a secondary control for all the mouse experiments, Ins-Cre mice were used, which were maintained by breeding female Ins-Cre mice with male $K8^{flox/-}$. Mice were genotyped as described previously (26). All mice were housed at the Central Animal Laboratory at the University of Turku (Turku, Finland) and handled according to the animal study licenses 197/04.10.07/2013, 3956/04.10.07/2016, ESAVI/16359/2019, and ESAVI/4498/2023, which were approved by the State Provincial Office of South Finland. Age-matched (2–6 mo) male and female mice were used as described in this study.

Streptozotocin Treatment

Streptozotocin (STZ) (Sigma-Aldrich, St. Louis, MO) dilution was prepared in 50 mM sodium citrate (Sigma-Aldrich) in PBS (pH 4.5) and administered intraperitoneally to mice in a single dose of 140 mg/kg. The blood glucose levels were measured from the tail vein, once on 4 h fasting before injection and once every day until 72 h postinjection. The mice were considered diabetic when two consecutive blood glucose measurements exceeded 14 mmol/L (28). Animals were euthanized 72 h after STZ administration and pancreas tissue samples were collected for further processing.

Histopathological Analysis

Pancreata from mice were dissected and fixed in paraformaldehyde (4% vol/vol in PBS, pH 7.4) for preparation of hematoxylin-eosin (H&E) stained paraffin-embedded sections. The sectioning and staining were performed at the Turku Center for Disease Modeling Histology Service Unit, University of Turku (Turku, Finland). A 40 μm sectioning interval was considered between each tissue section mounted on the slides. The sections were scanned using a Pannoramic 1000 system (3D HISTECH, Budapest, Hungary) and analyzed using QuPath 0.2.3 bioimage analysis software (29). To perform the histomorphological analysis, islets were annotated manually, and the islet mass was estimated by dividing the islet area to the tissue section area. For STZ-treated histopathological analysis, the islet damage was scored blinded, from 0 to 4, where 0 indicated no evident islet damage, 1 islet damage of 15%, 2 islet damage of 15–30%, 3 islet damage of 30–50%, and score 4 islet damage of >50%. A minimum of 40 islets per pancreas were scored.

Transmission Electron Microscopy and Image Analysis

Pancreata were dissected, and tissue pieces of 1–2 mm^2 were fixed in 5% glutaraldehyde in 0.16 mol/L S-collidin-HCl buffer, pH 7.4. Electron microscopy samples were processed in the Electron Microscopy Laboratory, Institute of Biomedicine, University of Turku, and islet β-cells were imaged using a JEM-1400 Plus transmission electron microscope (Jeol, Peabody, MA). The images were quantitatively analyzed using ImageJ software (National Institutes of Health, Bethesda, MD) for β-cell mitochondrial number and morphology. Mitochondria were manually annotated to measure the area. Cristae morphology was determined visually for individual mitochondria. The mitochondrial shape aspect ratio was determined by dviding the local height by local width.

Fasting Blood Glucose Measurements and Glucose and Insulin Tolerance Tests

Blood glucose levels were measured using a handheld glucose monitor (Contour, Bayer, Basel, Switzerland) by taking blood from the tail vein after fasting, and at indicated time intervals (up to 2.5 h) after a single intraperitoneal injection of 2 g/kg of body weight glucose (Sigma-Aldrich) or 0.75 U/kg

of body weight insulin (Liprolog, Oriola, Finland). Mice were fasted overnight for glucose tolerance tests and fasting blood glucose measurements, and for 4 h for the insulin tolerance tests.

Insulin Extraction from Pancreas Tissue

Pancreatic insulin content was determined by acid-ethanol extraction, using 1.5% vol./vol. concentrated HCl (Sigma-Aldrich, Saint Louis, MO) in 70% ethanol. Pancreata were dissected and tissue pieces from mid-pancreas were homogenized manually in 20 μL acid-ethanol solution/mg weight of pancreas tissue. The homogenate was incubated at 4°C overnight under stirring and then centrifuged at 13,000 *g* for 30 min. The supernatant containing extracted insulin was collected and stored at −80°C before further processing.

Glucose-Stimulated Insulin Secretion and Serum Insulin Measurement

Mice were challenged with 2 g/kg of body weight glucose (ip) after 4 h fasting. Blood was collected from fasted mice and 10 min after the glucose administration, from the femoral vein using a capillary blood sampling microvette (Sarstedt, Nümbrecht, Germany). Samples were centrifuged at 2,000 *g* for 10 min and serum was extracted to determine the insulin concentrations using a mouse ultrasensitive insulin enzyme-linked immunosorbent assay (ELISA) kit (Mercodia- 10-1247-01, Uppsala, Sweden) according to the manufacturer instructions.

Isolation of Pancreatic Islets

Pancreatic islets were isolated as previously described (30). Collagenase P (Roche, Mannheim, Germany) at concentration of 1.5 mg/mL, diluted in Hanks' Balanced Salt Solution (HBSS) (Sigma-Aldrich, Saint Louis, MO) was injected into the common bile duct for tissue digestion. Isolated islets were subsequently cultured in RPMI-1960 medium supplemented with 10% fetal bovine serum, 2 mM L-glutamine, and 100 U/mL penicillin-streptomycin at 37°C and 5% CO_2, for 24 h before further processing.

Dispase Assay

Isolated islets were stained with dithizone (Sigma-Aldrich) according to the supplier's instructions to confirm the exclusion of nonislet tissue. Islets were hand-picked under a dissection microscope (Leica MZ6), to collect islets of approximately similar size (including both smaller and larger islets) and achieve a roughly equal size distribution across groups. Islets were transferred to a 96-well plate (30 islets/well) with culture medium containing 17.5 U/mL dispase (Sigma-Aldrich). The plate was then placed on an orbital shaker to apply mechanical stress (250 rpm), at 37°C and 5% CO_2. After 3 h, the islet fragments and dissociated islet cells were imaged using bright-field Zeiss Axio Vert A1 microscope. The images were quantified for the number of intact islets and islet fragments using ImageJ software (National Institutes of Health, Bethesda, MD).

Cell Culture and Transfection

MIN6 cells (mycoplasma-free; AddexBio, San Diego, CA) were cultured in Dulbecco's modified Eagle medium (DMEM) containing 15% fetal bovine serum, 1 mM sodium pyruvate, 0.05 mM β-mercaptoethanol, 2 mM L-glutamine, 100 units/mL penicillin, and 100 μg/mL streptomycin. The cells were grown in T25 flasks (Sarstedt, Nümbrecht, Germany) at 37°C and 5% CO_2. The cells were transfected using electroporation as previously described (21). The transfection constructs used were *Krt8/Krt18*, a kind gift from Rudolf Leube (Aachen University, Aachen, Germany), and *Krt18 R90C*, a kind gift from Bishr Omary (Rutgers University, New Brunswick, NJ).

SDS-PAGE and Immunoblotting

Isolated pancreatic islets and MIN6 cells were harvested and homogenized on ice in homogenization buffer (0.187 M Tris-HCl, 3% SDS, and 5 mM EDTA, pH 6.8) using a syringe and a 30G needle (Henke Sass Wolf, Tuttlingen, Germany). Samples were then prepared for protein measurement using a Pierce BCA protein assay kit (Thermo Fisher Scientific, Waltham, MA) in 5 μg protein/10 μL sample ratio using 3× Laemmli sample buffer (30% glycerol, 3% SDS, 0.1875 M Tris-HCl (pH 6.8), 0.015% bromophenol blue and 3% β-mercaptoethanol). SDS-PAGE was performed and samples were analyzed by immunoblotting. Primary antibodies used were rat anti-K8 (Troma I; Developmental Studies Hybridoma Bank), rabbit anti-K7 (monoclonal/ERP17078, Abcam, Cambridge, UK), rabbit anti-K18 (Sigma-Aldrich), rabbit anti-amylase (Biorbyt, Cambridge, UK), mouse MitoProfile Total Oxphos human WB antibody cocktail (Abcam, Cambridge, UK), rabbit anti-MFN2 (Sigma-Aldrich), rabbit anti-TCHP (Biorbyt, Cambridge, UK), rabbit anti-OPA1, rabbit anti-cytochrome C (Cell Signaling Technologies), mouse anti-β-tubulin (Sigma Aldrich, St. Louis, MO), and rabbit anti-GAPDH (Abcam). The Secondary antibodies used were anti-rabbit IgG-HRP (Promega, Madison, WI), anti-rat IgG-HRP (Cytiva, UK and Cell Signaling Technology), and anti-mouse IgG-HRP (Cytiva, UK). See Supplemental Tables S1 and S2 for antibody details and Research Resource Identifier information. The HRP signal was detected using Amersham ECL Western blotting detection reagent (Cytiva, UK) or ECL plus (PerkinElmer, Waltham, MA). The immunoblotting results were quantified using ImageJ software (National Institutes of Health, Bethesda, MD) and normalized to protein loading controls.

Immunofluorescence Staining and Image Analysis

Pancreata, intestine, liver, and kidney from mice were dissected and embedded in Optimal Cutting Temperature compound (OCT, Tissue-Tek, Sakura Finetek Europe B.V., Alphen aan den Rijn, The Netherlands). The frozen tissue was sectioned in 6 μm thickness using Leica CM1950 Research Cryostat (Leica Microsystems, Wetzlar, Germany) and fixed in paraformaldehyde (1% vol./vol. in PBS, pH 7.4) or ice-cold acetone after which they were immunostained as previously described (31). Isolated islets were dispersed using trypsin and gentle pipetting motion, and MIN6 cells were plated on 10 mm glass coverslips and fixed in ice-cold acetone before staining. The primary antibodies used were rabbit anti-K7 (monoclonal/ERP17078, Abcam, UK), rat anti-K8 (Troma I; Developmental Studies Hybridoma Bank, Iowa, IA), rabbit anti-K18 (Sigma-Aldrich), mouse anti-K18 (Invitrogen), rabbit anti-insulin (Cell Signaling, Danvers, MA), mouse anti-insulin

(monoclonal; Santa Cruz Biotechnology, Dallas, TX), guinea pig anti-insulin (Progen, Heidelberg, Germany), mouse anti-glucagon (monoclonal; Santa Cruz Biotechnology), rabbit anti-GLUT2 (Millipore, Temecula, CA), rat anti-E-cadherin (Thermo Fisher Scientific, Waltham, MA), rabbit anti-Ki67 (Abcam, Cambridge, UK) and rabbit anti-YAP (Cell Signaling Technologies, Danvers, MA). The secondary antibodies used were donkey anti-rat Alexa 488 and 568, donkey anti-rabbit Alexa 488 and 546, goat anti-mouse Alexa 488, and goat anti-guinea pig Alexa 546 (Thermo Fisher Scientific, Waltham, MA). See Supplemental Tables S1 and S2 for antibody details and Research Resource Identifier information. DAPI (Invitrogen) and DRAQ5 (Thermo Fisher Scientific, Bannockburn, IL) were used for the nuclear staining and the stained tissue and cell samples were mounted using ProLong Gold antifade reagent (Invitrogen). All immunofluorescence-stained tissues and cells were imaged using Marianas Spinning disk confocal microscope (Intelligent Imaging Innovations, Denver, CO) and/or SP5 confocal microscope (TCS SP5; Leica). For quantitative image analysis, ImageJ software (National Institutes of Health, Bethesda, MD) and QuPath 0.2.3 bioimage analysis software (29) were used. All the fluorescence signal intensity measurements and GLUT2 signal intensity profiling were done as previously described (21). For quantitative analysis of cell membrane features using E-cadherin staining, cells were manually annotated and membrane roundness was normalized to cell shape aspect ratio according to (32). For tissue disorganization analysis, images were minimally preprocessed, and Voronoi analysis (33, 34) was applied while the tissue irregularity index was calculated by mean cell area divided by standard deviation (SD).

Statistical Analysis

Statistical analyses were performed using Prism 9 (GraphPad Software, San Diego, CA). Student's *t* test, one-way and two-way ANOVA, Fisher's exact test, and logarithmic analysis were used as indicated in the figure legends. Statistically significant differences are shown as $*P < 0.05$, $**P < 0.01$, $***P < 0.001$, or $****P < 0.0001$.

RESULTS

Loss of β-Cell K8 Leads to Decreased K18 Expression

To investigate the role of β-cell K8 in islet physiology and pathophysiology, we developed a β-cell specific K8 knockout mouse using conditional *Krt8* gene inactivation. We crossed $K8^{flox/flox}$ (26) and $Ins1^{Cre}$ (27) mice to achieve β-cell specific K8 deletion at the embryonic level (here called $K8^{flox/flox}$; Ins-Cre). Complete loss of β-cell K8 was confirmed in $K8^{flox/flox}$; Ins-Cre islets by K8 immunostaining of pancreatic tissue while K8 was still present in the surrounding exocrine pancreas (Fig. 1*Ab*) as expected. Immunostaining of dispersed islet cells from the $K8^{flox/flox}$; Ins-Cre mice confirmed that insulin-positive β-cells were devoid of K8 (Fig. 1*Bb*). Both islet tissue immunostaining, and immunoblotting of isolated islets showed a decrease in K18 protein levels (∼40%) in $K8^{flox/flox}$; Ins-Cre mice compared with $K8^{flox/flox}$ control (Fig. 1, *A*, *c–f*, *C*, and *D*). The remaining K18 expression was likely due to pairing and filament formation with K7. No significant overall change in K7 levels in $K8^{flox/flox}$; Ins-Cre β-cells was detected, indicating that K7 is likely not able to compensate for the loss of K8 expression in β-cells in a tissue-wide manner (Fig. 1, *A*, *g–h*, *C*, and *E*). Immunoblotting of $K8^{flox/flox}$; Ins-Cre isolated islet lysates showed a minor K8 band (Fig. 1*C*), which was expected due to the K8 expression in other islet cell types (8, 21). In addition, a minor exocrine contamination in the islet lysate samples was observed (evidenced by the presence of amylase), which likely also contributed to the K8 signal in all isolated islet samples (Fig. 1*C*). The K7, K8, and K18 islet expression in Ins-Cre control mice (Supplemental Fig. S1) was comparable to that of $K8^{flox/flox}$ mice (Fig. 1*A*). $K8^{flox/flox}$; Ins-Cre K8 and K18 were expressed at comparable levels to $K8^{flox/flox}$ in other major K8-expressing epithelial organs including the liver, kidney, and colon (Supplemental Fig. S2), further confirming the specific deletion of K8 from β-cells.

Loss of β-Cell K8 Does Not Alter the Pancreatic Islet Histomorphology

To investigate the effect of β-cell specific K8 loss on islet histomorphology, islet phenotype was assessed using H&E stained pancreas sections (Fig. 2*A*). No significant alterations in the islet mass (Fig. 2*B*), islet number (Fig. 2*C*) per pancreas tissue area, or mean islet size (Fig. 2*D*) was observed in $K8^{flox/flox}$; Ins-Cre mice compared with $K8^{flox/flox}$. The Ins-Cre gene insertion did not affect the islet histomorphology, as Ins-Cre mouse islet size, the frequency distribution of islet size, mass, and the islet number were comparable to $K8^{flox/flox}$ mice (Supplemental Fig. S3, *A–E*). To examine the proportions of islet cell types, we analyzed the islet α- and β-cell population ratio in $K8^{flox/flox}$; Ins-Cre dispersed islets immunostained for insulin and glucagon, respectively. We also assessed the level of active proliferation by the number of Ki67-positive cells in islet sections. Neither the α-to β-cell ratio nor the level of active cell proliferation in $K8^{flox/flox}$; Ins-Cre islets differed from $K8^{flox/flox}$ (Supplemental Fig. S3, *F* and *G*).

β-Cell K8 Maintains the Islet Tissue Integrity and Mechanical Stability

As K8 and K18 protect the colon and liver against tissue fragility (23, 35), we asked if β-cell K8 might similarly protect the mechanical integrity of islet tissue or islet cell adhesion properties. We observed that the number of islets isolated from $K8^{flox/flox}$; Ins-Cre and $K8^{flox/flox}$ mice pancreata after collagenase P digestion was similar (Fig. 3*A*). However, when islets exposed to the enzyme dispase were subjected to mechanical stress for 3 h, a higher number of islet cell fragments and a decrease in the number of intact islets could be observed in $K8^{flox/flox}$; Ins-Cre mice compared with $K8^{flox/flox}$ (Fig. 3, *B–D*). To investigate this further, we immunostained the pancreas tissue sections for cell adhesion protein E-cadherin (Fig. 3*E*), which is a well-characterized mechanosensor and mediator protein for β-cell adhesion and structure (36, 37). A significant disorganization of the β-cell plasma membrane, as well as islet tissue structure, evidenced by a decrease in β-cell membrane roundness and tissue structure regularity was observed in $K8^{flox/flox}$; Ins-Cre islets (Fig. 3, *F* and *G*). Moreover, membrane-proximal E-cadherin protein expression was reduced in $K8^{flox/flox}$;

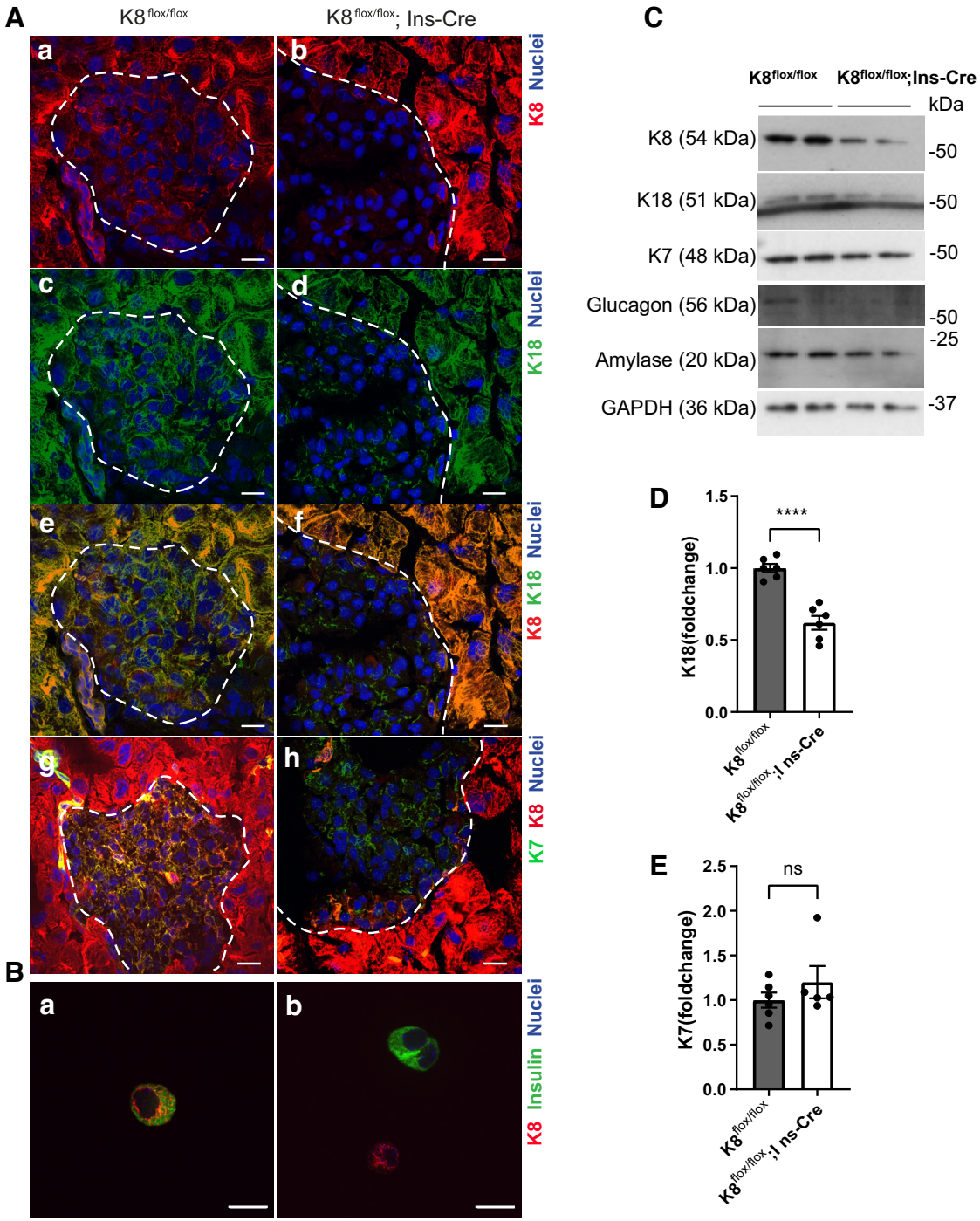

Figure 1. β-Cell K8 loss leads to decrease in K18 expression with no overall change in K7 expression in β-cells. *A*: immunostaining of pancreatic sections from K8$^{flox/flox}$ and K8$^{flox/flox}$; Ins-Cre mice for K8 (*a, b*), K18 (*c, d*), K8/K18 (*e, f*), and K7/K8 (*g, h*). *B*: immunostaining of dispersed islet cells isolated from K8$^{flox/flox}$ and K8$^{flox/flox}$; Ins-Cre mice for K8/insulin (*a, b*). Images represent $n = 3$ male mice per group. *C–E*: immunoblotting of isolated islets from K8$^{flox/flox}$ and K8$^{flox/flox}$; Ins-Cre mice for K8, K18, K7, glucagon, and amylase. The immunoblots for K18 (*D*) and K7 (*E*) were quantified and normalized to GAPDH (representative of $n = 10–12$ male mice with isolated islets from two mice combined in each lane). Scale bars = 20 μm (*A*) and 10 μm (*B*). Islets are indicated by dotted lines. Data are shown as means ± SE, and data analyzed using Student's *t* test, ns, not significant; ****$P < 0.0001$. MW (kDa) indicates the closest molecular weight marker on the Western blots, whereas the expected protein molecular weight is mentioned next to each protein name.

Ins-Cre β-cells (Fig. 3*H*). To investigate whether the decrease in β-cell membrane E-cadherin and islet tissue disorganization compromise the mechanical stability of β-cells and islet tissue, we performed immunostaining for the mechanosensor yes-associated protein (YAP) (Fig. 3*I*) (38, 39). Immunostaining indicated a slight, but significant increase of YAP accumulation in K8$^{flox/flox}$; Ins-Cre β-cell nuclei compared with the nuclei of K8$^{flox/flox}$ β-cells (Fig. 3*J*). Together, these results indicate a role for β-cell K8 in maintaining the islet tissue integrity and mechanical robustness.

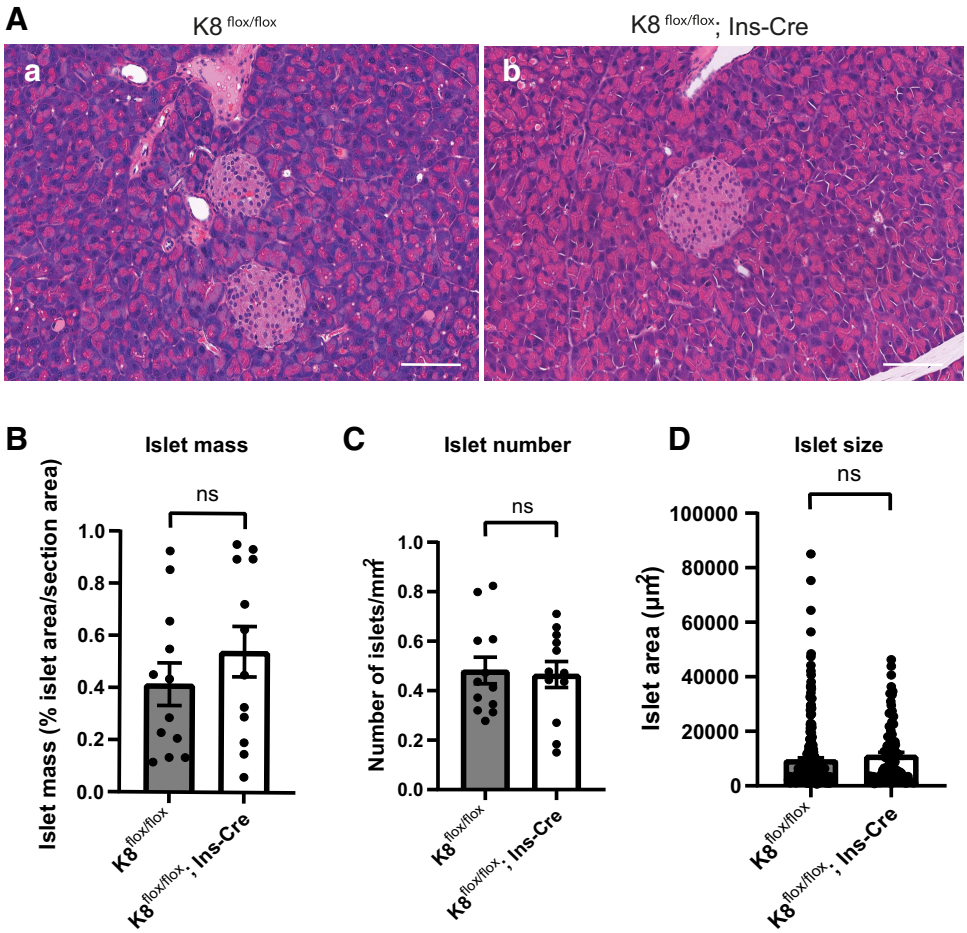

Figure 2. β-Cell K8 loss does not alter the basal islet histomorphology. *A*: pancreatic sections from $K8^{flox/flox}$ and $K8^{flox/flox}$; Ins-Cre mice (*a, b*) were analyzed using hematoxylin-eosin staining for (*B*) islet mass ($n = 12$ histological sections analyzed from three male mice per group). *C*: islet number ($n = 12$ histological sections analyzed from three male mice per group). *D*: islet size ($n = 97–258$ islets analyzed from three male mice per group). Scale bars = 100 µm, graph dots represent individual histological sections (*B*, *C*) and islets (*D*). Data are shown as means ± SE, and data analyzed using Student's *t* test (*B, C*) and Mann–Whitney's *U* test (*D*), ns, not significant.

β-Cell K8 Does Not Alter the Systemic Blood Glucose Regulation, but Modifies the β-Cell Glucose-Stimulated Insulin Response

Blood glucose homeostasis is dependent on β-cell function. Previously, a lower fasting blood glucose, higher glucose tolerance, and insulin sensitivity with a reduced pancreatic insulin content were reported in $K8^{-/-}$ mice (8). However, glucose uptake in hepatocytes and glycogen synthesis is increased in $K8^{-/-}$ mice (40), implying that systemic K8 loss may modulate blood glucose regulation through a concerted action of multiple organs. To determine the independent role of β-cell K8 in the physiological control of blood glucose and islet function, we investigated the systemic glycemic control in $K8^{flox/flox}$; Ins-Cre mice. No change was observed in the body weight (Fig. 4*A*), and the mice retained normal overnight fasting blood glucose levels compared with $K8^{flox/flox}$ (Fig. 4*B*). The pancreas tissue insulin content was also similar to that of $K8^{flox/flox}$ (Fig. 4*C*) and $K8^{flox/flox}$; Ins-Cre mice further demonstrated an unchanged glucose tolerance (Fig. 4*D*). On a short-term insulin challenge, $K8^{flox/flox}$; Ins-Cre mice were able to sustain a similar blood glucose regulation to $K8^{flox/flox}$ (Fig. 4*E*). Likewise, fasting serum insulin levels were not significantly different to $K8^{flox/flox}$ mice after a 4 h fast (Fig. 4*F*). However, when performing a glucose-stimulated insulin secretion (GSIS) test, intraperitoneal glucose administration did not induce any significant increase in serum insulin in $K8^{flox/flox}$; Ins-Cre mice, whilst $K8^{flox/flox}$ showed an increase in serum insulin levels 10 min after intraperitoneal glucose challenge, as expected (Fig. 4*F*). Control Ins-Cre mice were tested in an identical setting, and showed a similar systemic blood glucose regulation to $K8^{flox/flox}$ mice (Supplemental Fig. S4, *A–D*). These results show that β-cell K8 does not alter the systemic glycemic control, but may have a role in the regulation of insulin release in the GSIS process.

β-Cell K8 Maintains Mitochondrial Morphology, but Does Not Affect the Levels of Mitochondrial Regulatory or Functional Proteins

As mitochondrial function and ATP production are central for glucose-stimulated insulin secretion, we assessed if loss of β-cell K8 leads to mitochondrial alterations. Ultrastructural analysis of $K8^{flox/flox}$; Ins-Cre β-cell mitochondria (Fig. 5*A*) demonstrated a decrease in mitochondrial size with a higher percentage of small mitochondria (Fig. 5, *B* and *C*), and less electron-dense, more diffuse cristae (Fig. 5*D*). However, absence of β-cell K8 did not alter the total number of mitochondria per unit area (Fig. 5*E*) or mitochondrial shape (aspect ratio) (Fig. 5*F*). To investigate if the changes in mitochondrial size and cristae are related to alterations in the fission or fusion processes, or the levels of mitochondrial inner membrane proteins (41), we analyzed the levels of OPA1 and mitofusin 2 (MFN2), fusion regulatory proteins respectively

located on the inner and outer mitochondrial membranes (42). We also investigated the level of mitochondrial inner membrane proteins involved in oxidative phosphorylation, using immunoblotting of isolated islets. Protein levels of OPA1 and MFN2 (Fig. 5*G*), complex I (subunit NDUB8), III (subunit UQCRC2), IV (subunit COX2) and complex V (subunit ATP5A) and cellular cytochrome C were unaltered in $K8^{flox/flox}$; Ins-Cre islets compared with $K8^{flox/flox}$ (Fig. 5*H*).

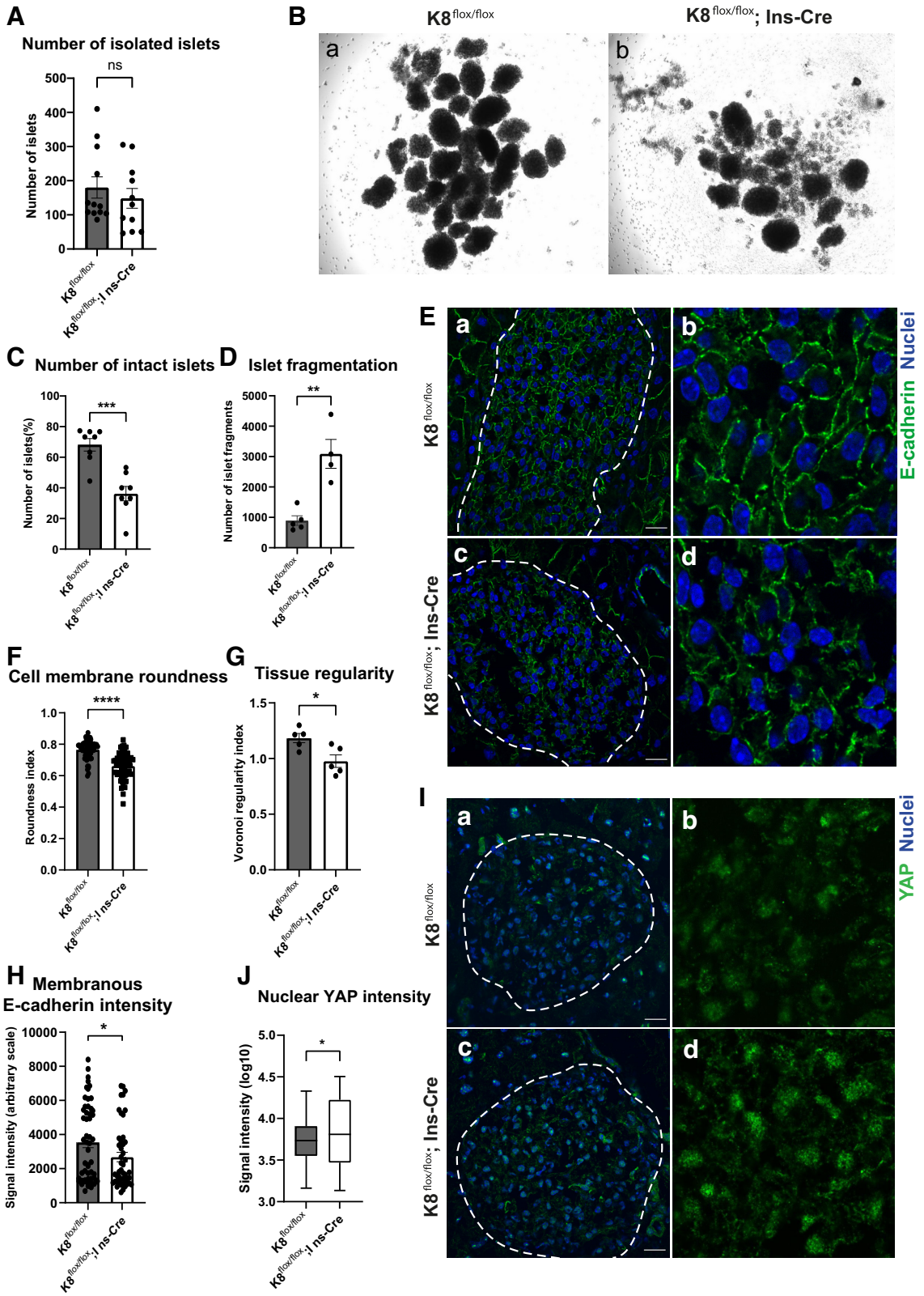

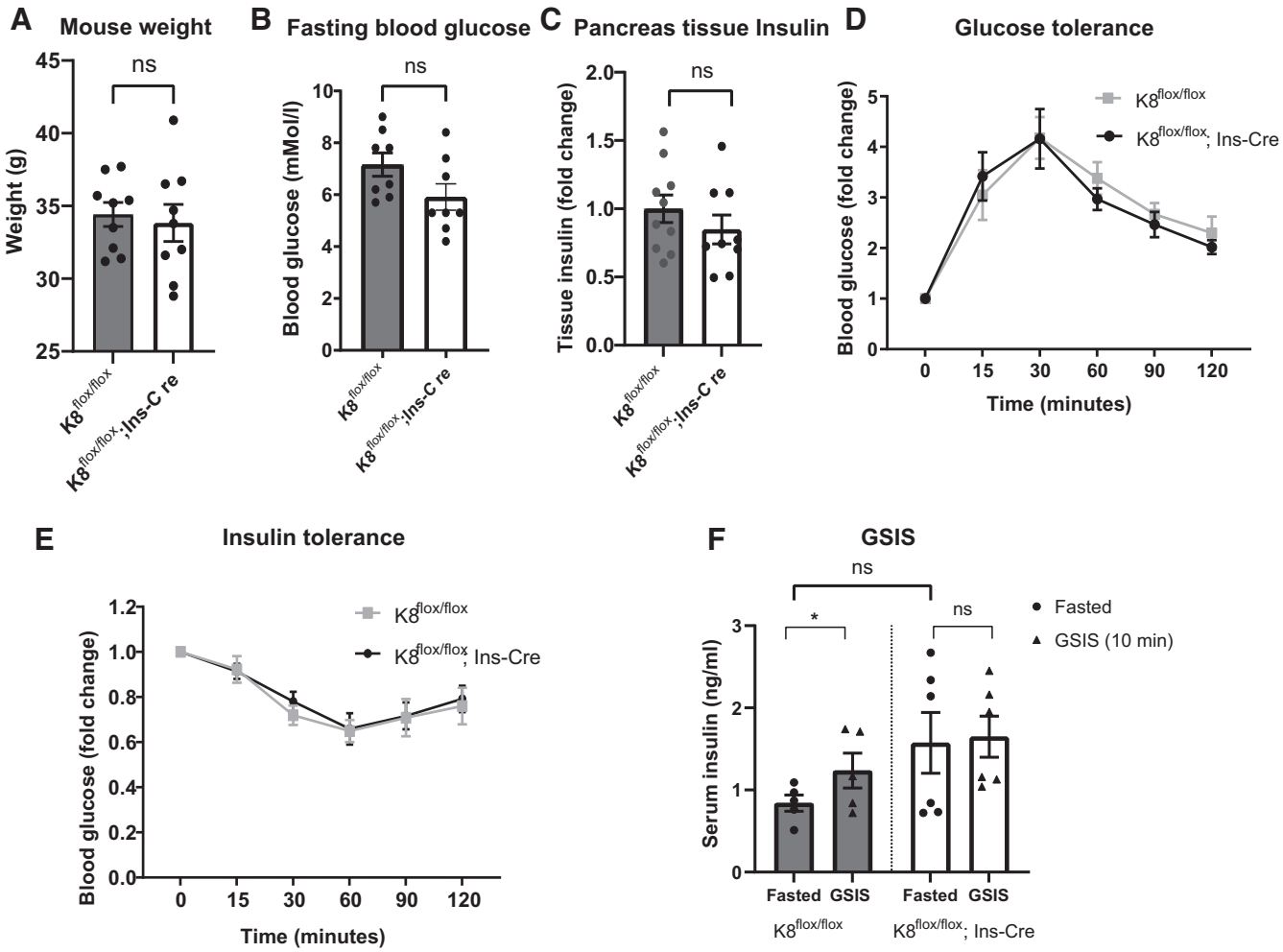

Figure 4. β-Cell K8 loss does not interfere with the systemic blood glucose regulation but leads to suppression of insulin response to glucose stimulation. $K8^{flox/flox}$ and $K8^{flox/flox}$; Ins-Cre mice were analyzed for (*A*) weight, (*B*) blood glucose levels after overnight fasting, (*C*) pancreas tissue insulin content, (*D*) glucose tolerance shown as blood glucose values as a function of time after glucose administration (intraperitoneal 2 g/kg of body weight), and (*E*) insulin tolerance shown as blood glucose values as a function of time after insulin administration (intraperitoneal insulin 0.75 U/kg of body weight). *F*: $K8^{flox/flox}$ and $K8^{flox/flox}$; Ins-Cre mice were analyzed for basal serum insulin and glucose-stimulated serum insulin levels (GSIS) 10 min after glucose administration (intraperitoneal 2 g/kg of body weight). $n = 6$–10 male mice per group, graph dots represent mice. Data are shown as means ± SE, and data analyzed using Student's *t* test (*A–C, F*) and two-way ANOVA (*D, E*), ns, not significant. $^*P < 0.05$.

The level of mitostatin (TCHP), a keratin-binding protein involved in mitochondrial dynamics (43) was also unchanged (Fig. 5*G*). These results demonstrate that β-cell K8 is likely involved in regulating mitochondrial morphology, but through mechanisms that are permissible to the mitochondrial fusion or oxidative phosphorylation.

β-Cell K8 Regulates the Cell Sensitivity toward Acute Toxic Effects of Streptozotocin

Keratins are upregulated in epithelial cells upon cell stress and tissue damage, and in disease conditions (12). To investigate the diabetes sensitivity in $K8^{flox/flox}$; Ins-Cre mice, a

Figure 3. β-Cell K8 maintains islet mechanical stability. *A*: quantification of number of islets isolated from $K8^{flox/flox}$ and $K8^{flox/flox}$; Ins-Cre mice ($n = 12$ male and female mice per group, each graph dot represents islets from two mice). *B*: isolated islets from $K8^{flox/flox}$ and $K8^{flox/flox}$; Ins-Cre mice (*a, b*) were exposed to enzyme dispase and subjected to mechanical stress under culture conditions 37°C and 5% CO_2 (images represent $n = 4$ male mice per group). Quantitative analysis of islet intactness (*C*) ($n = 8$ images analyzed from four male mice per group) and fragmentation (*D*) ($n = 5$ images analyzed from four male mice per group) for islets exposed to enzyme dispase and subjected to mechanical stress. *E*: immunostaining of pancreatic sections from $K8^{flox/flox}$ and $K8^{flox/flox}$; Ins-Cre mice (*a–d*) for E-cadherin (images represent $n = 3$ male mice per group). Quantitative analysis of β-cell membrane features for roundness (*F*) ($n = 60$ β-cells analyzed from three male mice per group), tissue regularity (*G*) ($n = 55$ β-cells analyzed from three male mice per group), and membranous E-cadherin signal intensity levels (*H*) ($n = 55$ β-cells analyzed from three male mice per group), *I*: Immunostaining of pancreatic sections from $K8^{flox/flox}$ and $K8^{flox/flox}$; Ins-Cre mice (*a–d*) for YAP (images represent $n = 4$ male mice per group) and *J*: quantitative analysis of YAP accumulation in nuclei ($n = 120$ cells analyzed from four male mice per group), boxes indicate 25–75 percentiles, line represent the median and whiskers show minimum and maximum values, graph dots represent islets (*A, C, G*), images (*D*) and β-cells (*F, H*). Scale bars = 20 μm, islets are indicated by dotted lines. Data are shown as means ± SE, and data analyzed using Student's *t* test, ns, not significant. $^*P < 0.05$, $^{**}P < 0.01$, $^{***}P < 0.001$, and $^{****}P < 0.0001$.

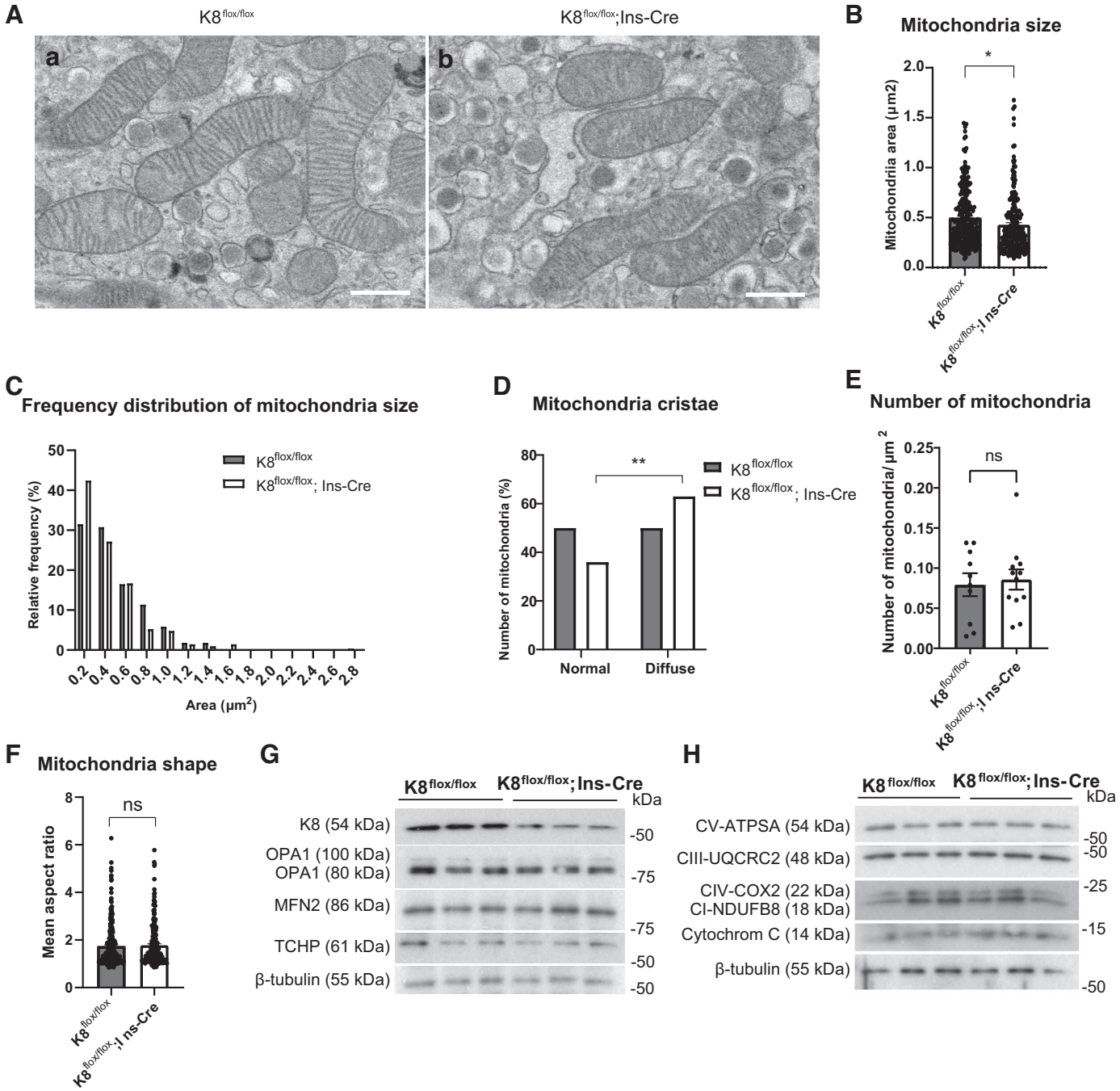

Figure 5. β-Cell K8 maintains mitochondrial size and cristae, but its loss does not affect the level of mitochondrial regulatory or functional proteins. *A*: transmission electron microscopy images of islet β-cells from K8$^{flox/flox}$ and K8$^{flox/flox}$; Ins-Cre mice (*a, b*) (images represent $n = 3$ male mice) were analyzed for mitochondria size ($n = 85–135$ mitochondria analyzed per group) (*B*), mitochondria size frequency distribution ($n = 85–135$ mitochondria analyzed per group) (*C*), morphology of mitochondria cristae ($n = 85–135$ mitochondria analyzed per group) (*D*), mitochondria number ($n = 10–12$ images analyzed from three male mice per group) (*E*), and mitochondria shape ($n = 85–135$ mitochondria analyzed per group) (*F*). *G*: immunoblotting of isolated islets from K8$^{flox/flox}$ and K8$^{flox/flox}$; Ins-Cre mice for K8, and mitochondrial regulatory proteins OPA1, MFN2, and TCHP (representative of $n = 12$ male mice with isolated islets from two mice combined in each lane), (*H*) immunoblotting of isolated islets from K8$^{flox/flox}$; Ins-Cre and K8$^{flox/flox}$ mice for oxidative phosphorylation protein complexes V (CV) subunit ATP5A, complex III (CIII) subunit UQCRC2, complex IV (CIV) subunit COX2, complex I (CI) subunit NDUFB8 and cytochrome *C*. Protein levels were normalized to β-tubulin (representative of $n = 12$ male mice with isolated islets from two mice combined in each lane). Scale bars = 500 nm. Data are shown as means ± SE, and data analyzed using Student's *t* test (*B, E*, and *F*) and Fisher's exact test (*D*), ns, not significant. $^*P < 0.05$ and $^{**}P < 0.01$. MW (kDa) indicates the closest molecular weight marker on the Western blots, whereas the expected protein molecular weight is mentioned next to each protein name.

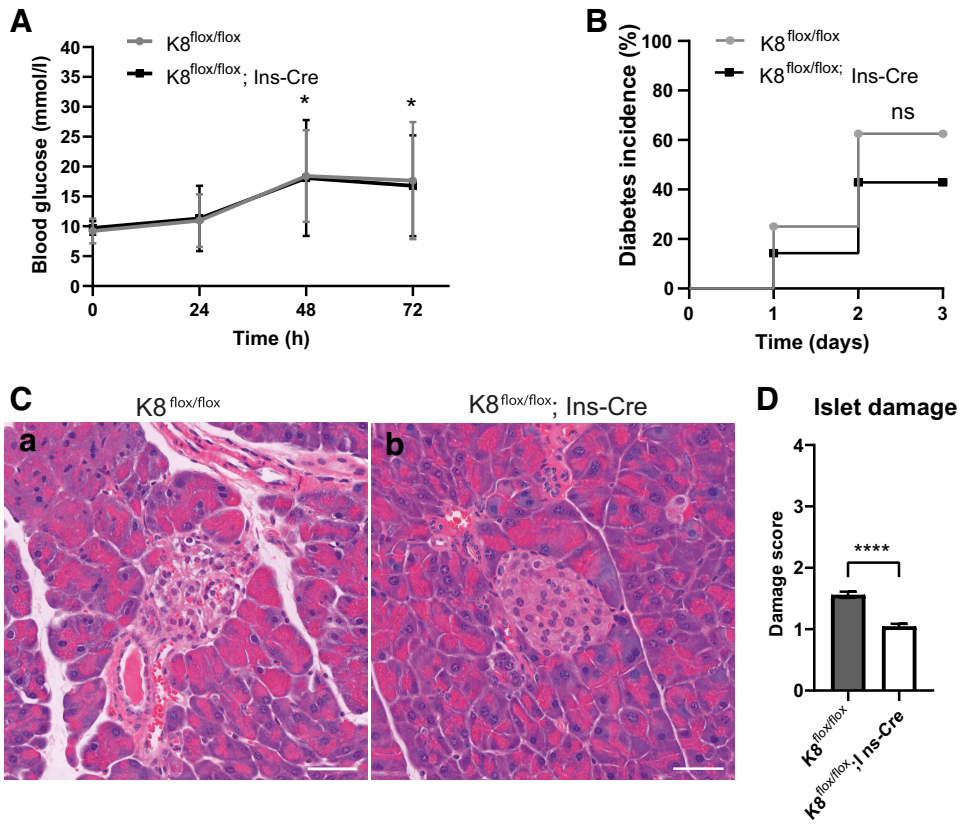

Figure 6. β-Cells without K8 are protected against acute toxic effects of STZ. *A*: blood glucose levels were analyzed in $K8^{flox/flox}$ and $K8^{flox/flox}$; Ins-Cre mice subjected to a single high-dose of STZ (intraperitoneal 140 mg/kg of body weight), (*B*) $K8^{flox/flox}$ and $K8^{flox/flox}$; Ins-Cre mice were assessed for diabetes incidence as a function of time with the blood glucose levels exceeding 14 mmol/L. ($n = 8$ male mice per group). *C*: pancreatic sections from $K8^{flox/flox}$ and $K8^{flox/flox}$; Ins-Cre mice (*a, b*) were analyzed using hematoxylin-eosin staining for islet damage (images represent $n = 8$ male mice per group) and (*D*) scored as islet cell loss of <15% (score 1), 15–30% (score 2), 30–50% (score 3) and >50% (score 4). Scale bars = 50 μm. Data are shown as means ± SE, and data analyzed using Student's *t* test, ns, not significant. $^*P < 0.05$ and $^{****}P < 0.0001$.

single high dose of the β-cell toxin; streptozotocin (STZ) was administered, and the blood glucose levels were monitored daily postinjection. Under these conditions a significant elevation in blood glucose levels was observed 48 and 72 h after STZ treatment in both $K8^{flox/flox}$; Ins-Cre and $K8^{flox/flox}$ mice (Fig. 6*A*), whereas only 43% of $K8^{flox/flox}$; Ins-Cre mice became diabetic (assessed by hyperglycemia ≥ 14 mmol/L) 48 h postinjection compared with 63% of $K8^{flox/flox}$ mice (Fig. 6*B*). Although this difference was not statistically significant, histopathological analysis showed significantly less islet damage in diabetic $K8^{flox/flox}$; Ins-Cre (Fig. 6, *C* and *D*) compared with $K8^{flox/flox}$ counterparts. When the islets were histologically scored (damage score 1–4), only 18.5% of $K8^{flox/flox}$ islets were intact compared with 31.2% of $K8^{flox/flox}$; Ins-Cre islets (Fig. 6*D*). These findings show that K8 deletion in β-cells renders the pancreatic islets less sensitive to the acute toxic effects of STZ.

β-Cell K8 Maintains the GLUT2 Plasma Membrane Localization

As STZ is taken up by β-cells via GLUT2 (44), the protection from STZ damage in $K8^{flox/flox}$; Ins-Cre mice could be due to a membrane-mislocalized GLUT2 hindering or delaying STZ uptake. To establish if β-cell K8 is responsible for the GLUT2 membrane-proximal localization, $K8^{flox/flox}$; Ins-Cre islet tissue was analyzed by immunostaining (Fig. 7*A*). GLUT2 fluorescent signal intensity profiled along a line drawn across the plasma membrane, connecting the nuclei of two adjacent β-cells, demonstrated a broader distribution of GLUT2 in the cytoplasm in $K8^{flox/flox}$; Ins-Cre β-cells compared with $K8^{flox/flox}$, in which GLUT2 was localized at the membrane between the two adjacent cells (Fig. 7, *A* and *B*). Although the mean cell GLUT2 level was unchanged, measured by the area under the signal distribution curve (AUC) (Fig. 7*D*), the analysis showed a significant decrease in the peak of GLUT2 fluorescence intensity over the cell membrane between the adjacent β-cells in $K8^{flox/flox}$; Ins-Cre compared with $K8^{flox/flox}$. These findings indicate decreased GLUT2 plasma membrane-proximal localization in the absence of β-cell K8 (Fig. 7*C*).

To further assess if K8 is required for GLUT2 membrane localization, we used mouse insulinoma MIN6 cells, which express minimal levels of endogenous filamentous keratins (21). To obtain K8/K18 filament formation, MIN6 cells were transiently transfected with human K8/K18 and immunostained for GLUT2. A significantly higher number (40%) of K8/K18 overexpressing MIN6 cells showed GLUT2 membrane-proximal localization compared with control cells devoid of keratin filaments, in which GLUT2 was more prominently distributed in the cytoplasm (Fig. 7, *Eb* and *F*). To explore whether intact K8/K18 filaments are needed for membrane GLUT2 targeting, we expressed human K8 with the filament assembly-deficient mutation K18R90C in MIN6 cells, which leads to a complete disassembly of the keratin filament network into dot-like structures (45) (Fig. 7*Ec*). Compared with intact human K8/K18 overexpressing MIN6 cells, there was a 35% decrease in membrane-proximal GLUT2 localization in cells with disrupted keratin filaments (Fig. 7*G*). Taken together, these results demonstrate that β-cell K8 maintains the GLUT2 plasma membrane localization and that an intact K8/K18 filament network is required for GLUT2 membrane targeting.

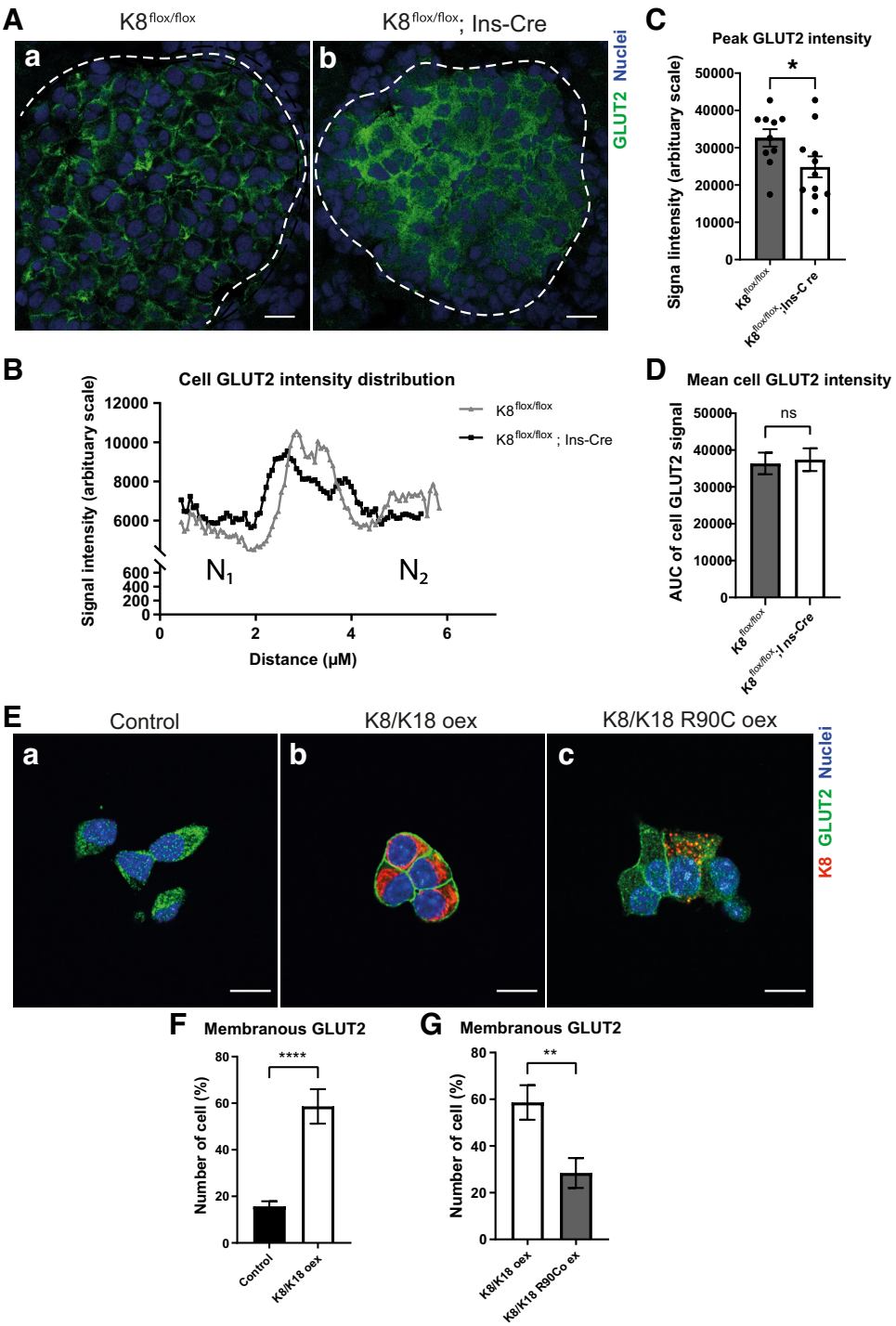

Figure 7. β-Cell K8 maintains the GLUT2 plasma membrane localization. *A*: immunostaining of pancreatic sections from $K8^{flox/flox}$ and $K8^{flox/flox}$; Ins-Cre mice for GLUT2 (images represent $n = 3$ male mice per group) were analyzed for (*B*) distribution of GLUT2 signal intensity across the plasma membrane of adjacent β-cell pairs by signal profiling on a line connecting the nuclei pair of β-cells ($n = 82$–88 β-cell pairs analyzed from three mice per group), (*C*) peak fluorescent intensity of GLUT2 across the plasma membrane of adjacent β-cell pairs ($n = 10$–11 β-cell pairs analyzed from three male mice per group) and (*D*) total cell GLUT2 content measured by the area under the curve (AUC) of average GLUT2 signal intensity distribution across the plasma membrane of adjacent β-cell pairs, (*E*) immunostaining of control MIN6 cells nearly devoid of keratin filaments (*a*), MIN6 cells overexpressing (oex) K8/K18 filaments (*b*), and MIN6 cells overexpressing K8/K18 R90C filament disrupting mutation (*c*) for GLUT2 (images represent $n = 3$). Quantitative analysis of membranous GLUT2 in MIN6 cells overexpressing K8/K18 filaments (*F*) and MIN6 cells overexpressing K8/K18 R90C filament disrupting mutation (*G*) ($n = 30$ cells analyzed per group). Scale bars = 20 μm (*A*) and 10 μm (*E*). Islets are indicated by dotted lines. Data are shown as means ± SE except in (*D*), which is shown as means ± SD, and data analyzed using Student's *t* test, ns, not significant, $*P < 0.05$, $**P < 0.01$, and $****P < 0.0001$.

DISCUSSION

In this study, we investigated for the first time the β-cell specific functions of the main IF protein K8 in vivo. The specific and complete β-cell K8 deletion in mice led to a significant reduction in the expression of its partnering type I keratin protein K18, with no significant overall compensatory upregulation of type II K7 protein. Here we report that β-cell K8 is required in vivo to maintain islet mechanical integrity and for the structural organization of essential functional β-cell proteins, including E-cadherin, YAP, and GLUT2. We further demonstrated the critical role of an intact K8/K18 filament network in vitro, for the membrane-targeting of GLUT2.

Previously, global $K8^{-/-}$ mice have been the only model used for studies related to the role of keratins in insulin/glucose processes (8, 40). Systemic K8 knockout, however, leads to a complicated physiological phenotype implying that multiorgan interactions (including the liver and intestine) contribute to the metabolic effects of K8 deletion (23, 46), making it difficult to discern the specific roles of β-cell K8 on

glucose- or insulin-related functions. Our results show that glucose-stimulated insulin release is blunted in the $K8^{flox/flox}$; Ins-Cre model similar to the $K8^{-/-}$ model (8). However, in $K8^{flox/flox}$; Ins-Cre mice, we did not note any differences in blood glucose regulation after glucose- or insulin challenge, indicating that despite a β-cell specific K8-dependent role in the GSIS response, blood glucose levels remain under control if K8 is expressed normally in other organs; the liver likely being the most important in this context (40).

Furthermore, impaired glucose-stimulated insulin responses in stem-cell-derived β-cells in vitro have been associated with YAP activation, as well as disturbed β-cell differentiation and proliferation (47). Although we did not observe any K8-related changes in cell type differentiation (α-/β-cell ratio) or proliferation in vivo in the islets, it is possible, that increased YAP activation in $K8^{flox/flox}$; Ins-Cre mouse β-cells contribute to the blunted GSIS response.

The keratin cytoskeleton is important for maintaining epithelial cell polarity and polarized membrane traffic (16, 48). Loss of K8 leads to mistargeting of polarized membrane proteins in other organs, such as the intestine (16). In vitro studies using hepatocyte and kidney cells overexpressing mutated K18R90C have demonstrated that this filament-disrupting mutation leads to disrupted E-cadherin membrane localization and increased cell size (49). Similar to other epithelial cells, β-cell functional membrane proteins are organized in a polarized manner: the β-cell surface is structured into specific functional domains where membrane proteins, including E-cadherin and GLUT2, accumulate at the lateral domains. This organization is thought to play a significant role in β-cell glucose and insulin responses (50–52).

E-cadherin is essential for cell-cell adhesion and contributes to several key cellular pathways, including mechanotransduction, cell growth, and development (36). E-cadherin also regulates YAP1 activation in keratinocytes and breast epithelial cells (53, 54). Isolated islets from $K8^{flox/flox}$; Ins-Cre mice in this study were more sensitive to combined enzymatic-mechanical disruption, and E-cadherin expression at the β-cell membrane was reduced and appeared disjointed, concomitant with the increased YAP nuclear localization. The keratin cytoskeleton in epithelial cells plays a major role in the maintenance of cell integrity and mechanical stability of the tissue (10). Hence, the increased nuclear accumulation of the mechanosensory YAP in β-cells could be associated with the β-cell fragility and the observed disorganization of β-cell membrane structure, which may disrupt the cell-cell contacts. Disruption of the membrane localization of proteins important in β-cell glucose uptake, polarity, and secretory function significantly alters β-cell function. This is evidenced by the increase in basal insulin secretion in MIN6 cells stably overexpressing E-cadherin (37). Therefore, our novel results strongly advocate a role for K8 in maintaining islet integrity and architecture in vivo and suggest that K8-dependent E-cadherin membrane localization may be a key contributor to these processes.

The impact of keratin deficiencies on tissue fragility in the liver and intestine has been studied extensively (17, 23), but the potential role of keratins in maintaining islet integrity in the pancreas has not previously been addressed. Due to the importance of islet integrity and architecture for susceptibility to T1D and in T2D pathology, a detailed understanding of the determinants regulating islet integrity is nevertheless critical (55). This insight is, moreover, directly applicable to islet isolation procedures for transplantation in diabetic patients, during which islets are exposed to considerable levels of mechanical and enzymatic stress.

β-Cell intracellular and functional robustness is important for counteracting insulin insufficiency (4). β-Cell function and the GSIS process are dependent on adequate cellular ATP levels (56, 57). Depending on the energetic state of the cell, the mitochondrial morphology and membrane composition change dynamically (25, 42, 58). Changes in mitochondrial size and networks have been reported in $K8^{-/-}$, K8 G62C, and K18 R90C mutation overexpressing mice, in hepatocytes and/or β-cells (25, 59). We show here that the mitochondria of β-cells with specific loss of K8 were smaller, with less electron-dense cristae which demonstrate a role for β-cell K8 in the regulation and maintenance of mitochondrial morphology. Decreased mitochondrial membrane surface area can compromise the activity and/or assembly of oxidative phosphorylation complexes (41), and a decrease in mitochondrial size can negatively impact the levels of energy metabolism (60), leading to insufficient mitochondrial function and ATP production. The decrease in mitochondrial size and electron-dense cristae in the absence of K8 can therefore be a contributing factor to the blunted insulin response to glucose stimulation that was observed in vivo in this study. As the levels of mitochondrial regulatory proteins OPA1, MFN2, and TCHP in isolated islets from $K8^{flox/flox}$; Ins-Cre mice were unchanged, the changes in mitochondrial network are unlikely to be related to the mitochondrial fission and fusion processes. Nevertheless, the decrease in $K8^{flox/flox}$; Ins-Cre β-cell K18 levels might contribute to the observed mitochondrial morphology changes, as K18 filament disruptions in vitro lead to smaller, more fragmented mitochondria (61). K18, moreover, reportedly contains an N-terminal amino acid sequence facilitating a direct interaction between keratin IFs and the outer mitochondrial membrane (62).

Another central factor that may affect GSIS is the alterations in the glucose transport processes. Loss of GLUT2 correlates with impairments in the GSIS process and changes in fasting blood glucose, as shown in several murine models of diabetes (2, 63, 64). Moreover, in human islets from diabetic donors, reduced GSIS is accompanied by a significant reduction in mRNA levels of GLUT1 and GLUT2 in β-cells (65). A major finding of the present study is that β-cell K8 is needed for GLUT2 plasma membrane localization both in vivo and in vitro. Glucose transporter membrane tethering has previously been associated with keratins in different organs. Keratin type II-knockout embryos show loss of plasma membrane GLUT1 and GLUT3 (66), and the global $K8^{-/-}$ mice display pronounced membrane mistargeting of GLUT2 in hepatocytes (40) and β-cells (8). Diabetes progression was, moreover, significantly altered in $K8^{-/-}$ mice subjected to acute and chronic STZ treatment (8). As the STZ mouse model of diabetes exhibits a broad spectrum of multiorgan damage, and considering the β-cell K8 role in GLUT2 cell membrane targeting as the gate for STZ uptake (44, 67), we investigated whether the lower diabetes incidence depends specifically on β-cell K8. We observed decreased diabetes incidence and less islet injury in $K8^{flox/flox}$; Ins-Cre mice after acute STZ treatment, concurrent with significantly decreased

GLUT2 β-cell plasma membrane localization, despite unaltered total β-cell GLUT2 protein levels. Similarly, in MIN6 cells a higher percentage of cells devoid of K8/K18 filaments, or overexpressing filament-disrupting K8/K18 R90C mutation, show mislocalization of GLUT2. Our results further demonstrate that GLUT2 localization at the cell membrane can be rescued in MIN6 cells by overexpressing K8/K18 filaments in these cells. Hence, using three different methods, our study demonstrates that β-cell K8 has a cell-type autonomous function in ensuring GLUT2 plasma membrane targeting.

It has been shown that elevated glucose levels in vitro lead to an increase in K8 protein levels as well as increased K8 acetylation and phosphorylation (24, 68, 69). Moreover, GLUT2 knockout mouse β-cells show a distinct loss of first-phase GSIS (70). Therefore, it can be speculated that the blunted GSIS response seen in $K8^{flox/flox}$; Ins-Cre mice, may be associated with the GLUT2 membrane mistargeting. Although the mechanisms behind GLUT2 membrane/cytoplasm trafficking have not been elucidated in detail, it is known that dysfunctional GLUT2 posttranslational modifications result in GLUT2 mislocalization from the β-cell surface (71). Hence, keratins could play a role in the regulations of GLUT2 posttranslational modifications in β-cells. However, further studies would be required to fully explore this possibility.

Conclusions

Our results demonstrate several previously unknown K8 functions in β-cells. This study underlines the importance of K8 filaments for the maintenance of β-cell ultrastructure, islet integrity, and β-cell mechanical stability, as well as β-cell plasma membrane protein targeting and organelle morphology. The results suggest that β-cell K8 is involved in the insulin response to glucose stimulation and modulates the sensitivity of β-cells to STZ-induced diabetes in mice. In addition, the β-cell autonomous roles of K8 in regulating cell membrane GLUT2 localization are demonstrated using mouse islet β-cells and MIN6 cells and we showed that K8 maintains β-cell robustness through the membrane targeting of the cell adhesion protein E-cadherin. It can be speculated that these mechanical and nonmechanical functions of K8 in β-cells may contribute to diabetes pathophysiology and underline the importance of this protein in maintaining β-cell structure and cellular processes that can directly or indirectly impact diabetes susceptibility.

DATA AVAILABILITY

The authors confirm that the data supporting the findings of this study are available within the article and the supplemental material links below.

SUPPLEMENTAL MATERIAL

Supplemental Figs. S1–S4: https://doi.org/10.23729/e4b86eb9-401e-4c35-9e7f-42baf2169058.

Supplemental Tables S1 and S2: https://doi.org/10.23729/7c2c9343-bc45-4f9f-866e-7e21cd1ce972.

ACKNOWLEDGMENTS

We are very grateful to Professor Karen M. Ridge (Northwestern University, USA) for donation of $K8^{flox/flox}$ transgenic mice. We thank all the members of Toivola Epithelial Biology Laboratory (Åbo Akademi University, Finland) especially Joel Nyström, Carl-Gustav Stenvall, Ahmed Al-Mosawi, and Taina Heikkilä for laboratory support. We are grateful to Dan S. Luciani (University of British Columbia, Canada) and Junel Solis (Turku BioImaging, Finland) for the fruitful discussions. We thank the personnel at the Central Animal Laboratory, University of Turku for their skillful technical support and Professor Rudolf Leube (RWTH Aachen University, Germany), and Professor Bishr Omary (Rutgers University, USA) for donating the plasmids. Imaging was performed at the Cell Imaging Core, Turku Bioscience Centre, Turku, Finland. Histology sample preparation was done at the Turku Center for Disease Modeling histology service unit, University of Turku, Finland, and electron microscopy samples were processed and imaged at the Electron Microscopy Laboratory, Institute of Biomedicine, University of Turku with the support of Biocenter Finland. The graphical abstract is created with BioRender.com.

GRANTS

This work was supported by the Novo Nordisk Foundation–NNF17OC002725/NNF20OC0063889, the Finnish Diabetes Research Foundation, the Sigrid Juselius Foundation, and Diabetes Wellness (to D.M.T.). This research also was supported by the Research Council of Finland's Flagship InFLAMES (337530 and 357910) and the EuroCellNet COST Action (CA15214), Swedish Cultural Foundation, Finnish Cultural Foundation, Jalmari and Rauha Ahokas Foundation, Paulo Foundation, Oskar Öflund Foundation, Waldemar von Frenckell Foundation, and Victoriastiftelsen.

DISCLOSURES

No conflicts of interest, financial or otherwise, are declared by the authors.

AUTHOR CONTRIBUTIONS

S.B., C.H., P.K., C.M.A., and D.M.T. conceived and designed research; S.B., C.H., P.K., C.M.A., and D.M.T. performed experiments; S.B., C.H., P.K., C.M.A., and D.M.T. analyzed data; S.B., C.H., P.K., C.M.A., and D.M.T. interpreted results of experiments; S.B., C.H., P.K., C.M.A., and D.M.T. prepared figures; S.B., C.M.A., and D.M.T. drafted manuscript; S.B., C.H., P.K., C.M.A., and D.M.T. edited and revised manuscript; S.B., C.H., P.K., C.M.A., and D.M.T. approved final version of manuscript.

REFERENCES

1. **Kaiser N**, **Leibowitz G**, **Nesher R.** Glucotoxicity and beta-cell failure in type 2 diabetes mellitus. *J Pediatr Endocrinol Metab* 16: 5–22, 2003. doi:10.1515/jpem.2003.16.1.5.
2. **Thorens B.** GLUT2, glucose sensing and glucose homeostasis. *Diabetologia* 58: 221–232, 2015. doi:10.1007/s00125-014-3451-1.
3. **Cerf ME.** Beta cell physiological dynamics and dysfunctional transitions in response to islet inflammation in obesity and diabetes. *Metabolites* 10: 452, 2020. doi:10.3390/metabo10110452.
4. **Chen C**, **Cohrs CM**, **Stertmann J**, **Bozsak R**, **Speier S.** Human beta cell mass and function in diabetes: recent advances in knowledge and technologies to understand disease pathogenesis. *Mol Metab* 6: 943–957, 2017. doi:10.1016/j.molmet.2017.06.019.
5. **Chang L**, **Chiang SH**, **Saltiel AR.** Insulin signaling and the regulation of glucose transport. *Mol Med* 10: 65–71, 2004. doi:10.2119/2005-00029.Saltiel.
6. **Arous C**, **Halban PA.** The skeleton in the closet: actin cytoskeletal remodeling in β-cell function. *Am J Physiol Endocrinol Physiol* 309: E611–E620, 2015. doi:10.1152/ajpendo.00268.2015.
7. **Bracey KM**, **Gu G**, **Kaverina I.** Microtubules in pancreatic β cells: convoluted roadways toward precision. *Front Cell Dev Biol* 10: 915206, 2022. doi:10.3389/fcell.2022.915206.

8. **Alam CM**, **Silvander JS**, **Daniel EN**, **Tao GZ**, **Kvarnström SM**, **Alam P**, **Omary MB**, **Hänninen A**, **Toivola DM.** Keratin 8 modulates β-cell stress responses and normoglycaemia. *J Cell Sci* 126: 5635–5644, 2013. doi:10.1242/jcs.132795.
9. **Schweizer J**, **Bowden PE**, **Coulombe PA**, **Langbein L**, **Lane EB**, **Magin TM**, **Maltais L**, **Omary MB**, **Parry DA**, **Rogers MA**, **Wright MW.** New consensus nomenclature for mammalian keratins. *J Cell Biol* 174: 169–174, 2006. doi:10.1083/jcb.200603161.
10. **Kim S**, **Coulombe PA.** Intermediate filament scaffolds fulfill mechanical, organizational, and signaling functions in the cytoplasm. *Genes Dev* 21: 1581–1597, 2007. doi:10.1101/gad.1552107.
11. **Jacob JT**, **Coulombe PA**, **Kwan R**, **Omary MB.** Types I and II keratin intermediate filaments. *Cold Spring Harb Perspect Biol* 10: a018275, 2018. doi:10.1101/cshperspect.a018275.
12. **Toivola DM**, **Strnad P**, **Habtezion A**, **Omary MB.** Intermediate filaments take the heat as stress proteins. *Trends Cell Biol* 20: 79–91, 2010. doi:10.1016/j.tcb.2009.11.004.
13. **Toivola DM**, **Polari L**, **Schwerd T**, **Schlegel N**, **Strnad P.** The keratin-desmosome scaffold of internal epithelia in health and disease – The plot is thickening. *Curr Opin Cell Biol* 86: 102282, 2024. doi:10.1016/j.ceb.2023.102282.
14. **Waschke J.** The desmosome and pemphigus. *Histochem Cell Biol* 130: 21–54, 2008. doi:10.1007/s00418-008-0420-0.
15. **Kumemura H**, **Harada M**, **Omary MB**, **Sakisaka S**, **Suganuma T**, **Namba M**, **Sata M.** Aggregation and loss of cytokeratin filament networks inhibit golgi organization in liver-derived epithelial cell lines. *Cell Motil Cytoskeleton* 57: 37–52, 2004. doi:10.1002/cm.10152.
16. **Toivola DM**, **Tao GZ**, **Habtezion A**, **Liao J**, **Omary MB.** Cellular integrity plus: organelle-related and protein-targeting functions of intermediate filaments. *Trends Cell Biol* 15: 608–617, 2005. doi:10.1016/j.tcb.2005.09.004.
17. **Omary MB**, **Ku NO**, **Strnad P**, **Hanada S.** Toward unraveling the complexity of simple epithelial keratins in human disease. *J Clin Invest* 119: 1794–1805, 2009. doi:10.1172/JCI37762.
18. **Alam CM**, **Baghestani S**, **Toivola DM.** Intermediate filament keratins in the exocrine pancreas. In: *Pancreapedia: Exocrine Pancreas Knowledge Base (e-Book)* (Gorelick FS, Williams JA, eds). American Pancreatic Association, 2020. Chapter 5, p. 72–84. doi:10.3998/panc.2020.02.
19. **Moll R**, **Divo M**, **Langbein L.** The human keratins: biology and pathology. *Histochem Cell Biol* 129: 705–733, 2008. doi:10.1007/s00418-008-0435-6.
20. **Toivola DM**, **Boor P**, **Alam C**, **Strnad P.** Keratins in health and disease. *Curr Opin Cell Biol* 32: 73–81, 2015. doi:10.1016/j.ceb.2014.12.008.
21. **Alam CM**, **Baghestani S**, **Pajari A**, **Omary MB**, **Toivola DM.** Keratin 7 is a constituent of the keratin network in mouse pancreatic islets and is upregulated in experimental diabetes. *Int J Mol Sci* 22: 7784, 2021. doi:10.3390/ijms22157784.
22. **Omary MB.** "IF-Pathies": a broad spectrum of intermediate filament–associated diseases. *J Clin Invest* 119: 1756–1762, 2009. doi:10.1172/JCI39894.
23. **Polari L**, **Alam CM**, **Nyström JH**, **Heikkilä T**, **Tayyab M**, **Baghestani S**, **Toivola DM.** Keratin intermediate filaments in the colon: guardians of epithelial homeostasis. *Int J Biochem Cell Biol* 129: 105878, 2020. doi:10.1016/j.biocel.2020.105878.
24. **Roux A**, **Gilbert S**, **Loranger A**, **Marceau N.** Impact of keratin intermediate filaments on insulin-mediated glucose metabolism regulation in the liver and disease association. *FASEB J* 30: 491–502, 2016. doi:10.1096/fj.15-277905.
25. **Silvander JSG**, **Kvarnström SM**, **Kumari-Ilieva A**, **Shrestha A**, **Alam CM**, **Toivola DM.** Keratins regulate β-cell mitochondrial morphology, motility, and homeostasis. *FASEB J* 31: 4578–4587, 2017. doi:10.1096/fj.201700095R.
26. **Stenvall CA**, **Tayyab M**, **Grönroos TJ**, **Ilomäki MA**, **Viiri K**, **Ridge KM**, **Polari L**, **Toivola DM.** Targeted deletion of keratin 8 in intestinal epithelial cells disrupts tissue integrity and predisposes to tumorigenesis in the colon. *Cell Mol Life Sci* 79: 10, 2021. doi:10.1007/s00018-021-04081-5.
27. **Thorens B**, **Tarussio D**, **Maestro MA**, **Rovira M**, **Heikkilä E**, **Ferrer J.** Ins1 (Cre) knock-in mice for beta cell-specific gene recombination. *Diabetologia* 58: 558–565, 2015. doi:10.1007/s00125-014-3468-5.
28. **Engkilde K**, **Buschard K**, **Hansen AK**, **Menné T**, **Johansen JD.** Prevention of diabetes in NOD mice by repeated exposures to a contact allergen inducing a sub-clinical dermatitis. *PLoS OnE* 5: e10591, 2010. doi:10.1371/journal.pone.0010591.
29. **Bankhead P**, **Loughrey MB**, **Fernández JA**, **Dombrowski Y**, **McArt DG**, **Dunne PD**, **McQuaid S**, **Gray RT**, **Murray LJ**, **Coleman HG**, **James JA**, **Salto-Tellez M**, **Hamilton PW.** QuPath: open source software for digital pathology image analysis. *Sci Rep* 7: 16878, 2017. doi:10.1038/s41598-017-17204-5.
30. **Zmuda EJ**, **Powell CA**, **Hai T.** A method for murine islet isolation and subcapsular kidney transplantation. *J Vis Exp* 50: 2096, 2011. doi:10.3791/2096.
31. **Ku NO**, **Toivola DM**, **Zhou Q**, **Tao GZ**, **Zhong B**, **Omary MB.** Studying simple epithelial keratins in cells and tissues. *Methods Cell Biol* 78: 489–517, 2004. doi:10.1016/s0091-679X(04)78017-6.
32. **Takashimizu Y**, **Iiyoshi M.** New parameter of roundness R: circularity corrected by aspect ratio. *Prog. Earth Planet. Sci* 3: 2, 2016. doi:10.1186/s40645-015-0078-x.
33. **Ogniewicz RL**, **Kübler O.** Hierarchic voronoi skeletons. *Pattern Recognit* 28: 343–359, 1995. doi:10.1016/0031-3203(94)00105-U.
34. **Su Y**, **Wu Y**, **Ji W**, **Sun X.** Computational morphogenesis of free-form grid structures with voronoi diagram. *Computer aided Civil Eng* 36: 318–330, 2021. doi:10.1111/mice.12621.
35. **Ku NO**, **Omary MB.** A disease- and phosphorylation-related nonmechanical function for keratin 8. *J Cell Biol* 174: 115–125, 2006. doi:10.1083/jcb.200602146.
36. **Bhatt T**, **Rizvi A**, **Batta SP**, **Kataria S**, **Jamora C.** Signaling and mechanical roles of E-cadherin. *Cell Commun Adhes* 20: 189–199, 2013. doi:10.3109/15419061.2013.854778.
37. **Carvell MJ**, **Marsh PJ**, **Persaud SJ**, **Jones PM.** E-cadherin interactions regulate beta-cell proliferation in islet-like structures. *Cell Physiol Biochem* 20: 617–626, 2007. doi:10.1159/000107545.
38. **Cai X**, **Wang KC**, **Meng Z.** Mechanoregulation of YAP and TAZ in cellular homeostasis and disease progression. *Front Cell Dev Biol* 9: 673599, 2021. doi:10.3389/fcell.2021.673599.
39. **Uttagomol J**, **Ahmad US**, **Rehman A**, **Huang Y**, **Laly AC**, **Kang A**, **Soetaert J**, **Chance R**, **Teh MT**, **Connelly JT**, **Wan H.** Evidence for the desmosomal cadherin desmoglein-3 in regulating YAP and phospho-YAP in keratinocyte responses to mechanical forces. *Int J Mol Sci* 20: 6221, 2019. doi:10.3390/ijms20246221.
40. **Mathew J**, **Loranger A**, **Gilbert S**, **Faure R**, **Marceau N.** Keratin 8/18 regulation of glucose metabolism in normal versus cancerous hepatic cells through differential modulation of hexokinase status and insulin signaling. *Exp Cell Res* 319: 474–486, 2013. doi:10.1016/j.yexcr.2012.11.011.
41. **Cogliati S**, **Frezza C**, **Soriano ME**, **Varanita T**, **Quintana-Cabrera R**, **Corrado M**, **Cipolat S**, **Costa V**, **Casarin A**, **Gomes LC**, **Perales-Clemente E**, **Salviati L**, **Fernandez-Silva P**, **Enriquez JA**, **Scorrano L.** Mitochondrial cristae shape determines respiratory chain supercomplexes assembly and respiratory efficiency. *Cell* 155: 160–171, 2013. doi:10.1016/j.cell.2013.08.032.
42. **Hoppins S.** The regulation of mitochondrial dynamics. *Curr Opin Cell Biol* 29: 46–52, 2014 [Erratum in Curr Opin Cell Biol 29:143, 2014]. doi:10.1016/j.ceb.2014.03.005.
43. **Nishizawa M**, **Izawa I**, **Inoko A**, **Hayashi Y**, **Nagata K**, **Yokoyama T**, **Usukura J**, **Inagaki M.** Identification of trichoplein, a novel keratin filament-binding protein. *J Cell Sci* 118: 1081–1090, 2005. doi:10.1242/jcs.01667.
44. **Hosokawa M**, **Dolci W**, **Thorens B.** Differential sensitivity of GLUT1- and GLUT2-expressing beta cells to streptozotocin. *Biochem Biophys Res Commun* 289: 1114–1117, 2001. doi:10.1006/bbrc.2001.6145.
45. **Ku NO**, **Michie SA**, **Soetikno RM**, **Resurreccion EZ**, **Broome RL**, **Oshima RG**, **Omary MB.** Susceptibility to hepatotoxicity in transgenic mice that express a dominant-negative human keratin 18 mutant. *J Clin Invest* 98: 1034–1046, 1996. doi:10.1172/JCI118864.
46. **Ku NO**, **Strnad P**, **Zhong BH**, **Tao GZ**, **Omary MB.** Keratins let liver live: mutations predispose to liver disease and crosslinking generates Mallory-Denk bodies. *Hepatology* 46: 1639–1649, 2007. doi:10.1002/hep.21976.
47. **Rosado-Olivieri EA**, **Anderson K**, **Kenty JH**, **Melton DA.** YAP inhibition enhances the differentiation of functional stem cell-derived insulin-producing β cells. *Nat Commun* 10: 1464, 2019. doi:10.1038/s41467-019-09404-6.
48. **Salas PJ**, **Forteza R**, **Mashukova A.** Multiple roles for keratin intermediate filaments in the regulation of epithelial barrier function and

apico-basal polarity. *Tissue Barriers* 4: e1178368, 2016. doi:10.1080/21688370.2016.1178368.

49. **Hanada S**, **Harada M**, **Kumemura H**, **Omary MB**, **Kawaguchi T**, **Taniguchi E**, **Koga H**, **Yoshida T**, **Maeyama M**, **Baba S**, **Ueno T**, **Sata M.** Keratin-containing inclusions affect cell morphology and distribution of cytosolic cellular components. *Exp Cell Res* 304: 471–482, 2005. doi:10.1016/j.yexcr.2004.12.009.
50. **Cottle L**, **Gan WJ**, **Gilroy I**, **Samra JS**, **Gill AJ**, **Loudovaris T**, **Thomas HE**, **Hawthorne WJ**, **Kebede MA**, **Thorn P.** Structural and functional polarisation of human pancreatic beta cells in islets from organ donors with and without type 2 diabetes. *Diabetologia* 64: 618–629, 2021. doi:10.1007/s00125-020-05345-8.
51. **Gan WJ**, **Zavortink M**, **Ludick C**, **Templin R**, **Webb R**, **Webb R**, **Ma W**, **Poronnik P**, **Parton RG**, **Gaisano HY**, **Shewan AM**, **Thorn P.** Cell polarity defines three distinct domains in pancreatic β Cells. *J. Cell Sci* 130: 143–151, 2016. doi:10.1242/jcs.185116.
52. **Geron E**, **Boura-Halfon S**, **Schejter ED**, **Shilo BZ.** The edges of pancreatic islet β cells constitute adhesive and signaling microdomains. *Cell Rep* 10: 317–325, 2015. doi:10.1016/j.celrep.2014.12.031.
53. **Kim NG**, **Koh E**, **Chen X**, **Gumbiner BM.** E-cadherin mediates contact inhibition of proliferation through hippo signaling-pathway components. *Proc Natl Acad Sci USA* 108: 11930–11935, 2011. doi:10.1073/pnas.1103345108.
54. **Schlegelmilch K**, **Mohseni M**, **Kirak O**, **Pruszak J**, **Rodriguez JR**, **Zhou D**, **Kreger BT**, **Vasioukhin V**, **Avruch J**, **Brummelkamp TR**, **Camargo FD.** Yap1 acts downstream of α-catenin to control epidermal proliferation. *Cell* 144: 782–795, 2011. doi:10.1016/j.cell.2011.02.031.
55. **Adams MT**, **Blum B.** Determinants and dynamics of pancreatic islet architecture. *Islets* 14: 82–100, 2022. doi:10.1080/19382014.2022.2030649.
56. **Giacomello M**, **Pyakurel A**, **Glytsou C**, **Scorrano L.** The cell biology of mitochondrial membrane dynamics. *Nat Rev Mol Cell Biol* 21: 204–224, 2020. doi:10.1038/s41580-020-0210-7.
57. **Jitrapakdee S**, **Wutthisathapornchai A**, **Wallace JC**, **MacDonald MJ.** Regulation of insulin secretion: role of mitochondrial signalling. *Diabetologia* 53: 1019–1032, 2010. doi:10.1007/s00125-010-1685-0.
58. **Maechler P.** Mitochondrial function and insulin secretion. *Mol Cell Endocrinol* 379: 12–18, 2013. doi:10.1016/j.mce.2013.06.019.
59. **Tao GZ**, **Looi KS**, **Toivola DM**, **Strnad P**, **Zhou Q**, **Liao J**, **Wei Y**, **Habtezion A**, **Omary MB.** Keratins modulate the shape and function of hepatocyte mitochondria: a mechanism for protection from apoptosis. *J Cell Sci* 122: 3851–3855, 2009. doi:10.1242/jcs.051862.
60. **Chen H**, **Chomyn A**, **Chan DC.** Disruption of fusion results in mitochondrial heterogeneity and dysfunction. *J Biol Chem* 280: 26185–26192, 2005. doi:10.1074/jbc.M503062200.
61. **Kumemura H**, **Harada M**, **Yanagimoto C**, **Koga H**, **Kawaguchi T**, **Hanada S**, **Taniguchi E**, **Ueno T**, **Sata M.** Mutation in keratin 18 induces mitochondrial fragmentation in liver-derived epithelial cells. *Biochem Biophys Res Commun* 367: 33–40, 2008. doi:10.1016/j.bbrc.2007.12.116.
62. **Chernoivanenko IS**, **Matveeva EA**, **Gelfand VI**, **Goldman RD**, **Minin AA.** Mitochondrial membrane potential is regulated by vimentin intermediate filaments. *FASEB J* 29: 820–827, 2015. doi:10.1096/fj.14-259903.
63. **Hou JC**, **Williams D**, **Vicogne J**, **Pessin JE.** The glucose transporter 2 undergoes plasma membrane endocytosis and lysosomal degradation in a secretagogue-dependent manner. *Endocrinology* 150: 4056–4064, 2009. doi:10.1210/en.2008-1685.
64. **Santer R**, **Schneppenheim R**, **Suter D**, **Schaub J**, **Steinmann B.** Fanconi-bickel syndrome - the original patient and his natural history, historical steps leading to the primary defect, and a review of the literature. *Eur J Pediatr* 157: 783–797, 1998. doi:10.1007/s004310050937.
65. **Del Guerra S**, **Lupi R**, **Marselli L**, **Masini M**, **Bugliani M**, **Sbrana S**, **Torri S**, **Pollera M**, **Boggi U**, **Mosca F**, **Del Prato S**, **Marchetti P.** Functional and molecular defects of pancreatic islets in human type 2 diabetes. *Diabetes* 54: 727–735, 2005. doi:10.2337/diabetes.54.3.727.
66. **Vijayaraj P**, **Kröger C**, **Reuter U**, **Windoffer R**, **Leube RE**, **Magin TM.** Keratins regulate protein biosynthesis through localization of GLUT1 and -3 upstream of AMP kinase and raptor. *J Cell Biol* 187: 175–184, 2009. doi:10.1083/jcb.200906094.
67. **Ku NO**, **Toivola DM**, **Strnad P**, **Omary MB.** Cytoskeletal keratin glycosylation protects epithelial tissue from injury. *Nat Cell Biol* 12: 876–885, 2010. doi:10.1038/ncb2091.
68. **Ahmed M**, **Bergsten P.** Glucose-induced changes of multiple mouse islet proteins analysed by two-dimensional gel electrophoresis and mass spectrometry. *Diabetologia* 48: 477–485, 2005. doi:10.1007/s00125-004-1661-7.
69. **Wen F**, **Xia Q**, **Zhang H**, **Shia H**, **Rajesh A**, **Wu Y**, **Yang Y**, **Yang Z.** Resistin activates p65 pathway and reduces glycogen content through keratin 8. *Int J Endocrinol* 2020: 9767926, 2020. doi:10.1155/2020/9767926.
70. **Guillam MT**, **Hümmler E**, **Schaerer E**, **Yeh JI**, **Birnbaum MJ**, **Beermann F**, **Schmidt A**, **Dériaz N**, **Thorens B.** Early diabetes and abnormal postnatal pancreatic islet development in mice lacking glut-2. *Nat Genet* 17: 327–330, 1997 [Erratum in Nat Genet 17: 503, 1997]. doi:10.1038/ng1197-327.
71. **Ohtsubo K**, **Takamatsu S**, **Minowa MT**, **Yoshida A**, **Takeuchi M**, **Marth JD.** Dietary and genetic control of glucose transporter 2 glycosylation promotes insulin secretion in suppressing diabetes. *Cell* 123: 1307–1321, 2005. doi:10.1016/j.cell.2005.09.041.